RESEARCH ARTICLE

INTERNATIONAL RESEARCH JOURNAL OF MULTIDISCIPLINARY TECHNOVATION

Asian Research Association

DOI: 10.54392/irjmt24312

PV based Systems with Advanced Control Strategies for Load Balancing in Multilevel Inverter

R. Venkedesh [a,*], R. Anandha Kumar [a], G. Renukadevi [b]

[a] Department of Electrical Engineering, Annamalai University, Chidambaram-608002, Tamil Nadu, India

[b] Department of Robotics & Automation, Manakula Vinayagar Institute of Technology, Pondicherry- 605107, India.

*Corresponding Author Email: venkrv@gmail.com

DOI: https://doi.org/10.54392/irjmt24312

Received: 14-12-2023; Revised: 17-04-2024; Accepted: 30-04-2024; Published: 14-05-2024

Abstract: In an era driven by sustainable energy solutions, the synergy of photovoltaic (PV) system stands as a beacon of hope for meeting the world's growing energy demands while minimizing environmental impact. This research ventures into the domain of renewable energy integration by seamlessly including a PV system, ingeniously controlled by Chaotic Flower Pollination Optimized Adaptive Neuro Fuzzy Inference System (ANFIS) based MPPT (Maximum Power Point Tracking) controller capable of optimizing the efficiency in the face of ever-changing weather dynamics. The PV system's quest for optimal efficiency receives a substantial boost through the implementation of the High Gain Modified Luo Converter. Designed to achieve an optimal PV output voltage, this converter's prowess finds its true calling in grid applications, where precision and efficiency are paramount. Furthermore, this research extends its purview to incorporate a bidirectional converter linked to an energy storage solution, such as a battery, through a common DC link. The output power is then passed to the Flyback Converter, seamlessly connected to a 31 level Cascaded H Bridge Multi-Level Inverter (31-level CHB MLI) controlled by PI controller. This formidable inverter architecture facilitates the efficient delivery of power to the grid, ensuring a smooth and controlled integration of renewable energy resources. This strategic integration bolsters the system's adaptability, enabling the seamless management of energy flows and grid interactions along with load balancing in MLI. The MATLAB simulation platform is used for confirming the system's overall performance. According to the simulation results, the proposed approach achieves the maximum efficiency with the lowest THD value of 94.5% and 2.5%, respectively.

Keywords: PV System, Chaotic Flower Pollination Optimized ANFIS based MPPT, High Gain Modified Luo converter, Fly back converter, 31-level CHB MLI

1. Introduction

In recent years, especially home and industrial applications for energy from sustainable sources have increased considerably [1]. The grid's ability to successfully integrate solar PV has been continuously prospering, yet it has certain effects on the amount of electricity is produced [2]. PV module's main goal is to make sure every module operates as well as possible when exposed to a variety of climatic variables brought on by variations in irradiance levels and shifts in ambient temperature [3, 4]. The DC to DC converter is employed to improve the minimal DC voltage source because it provides flexible input and output voltage shift ratios, rapid current and voltage regulation [5]. To increase the DC voltage gain as needed, a variety of DC-DC converters are offered in the electronics sector. Straightforward interconnection of the grid integrated PV system Mentioned in to the supercapacitor battery HSS. The lifespan of the ESS possibly increased by implementing the suggested control technique. Due to a restriction on the DC-link voltage changes, the MPPT is still not utilised when the reference voltage is lower than the battery voltage. Cascaded multilevel converter, which is proposed in reference, improves the reliability of single-phase grid linked PV systems during partial shading [6]. It also satisfies the requirements of partial shading conditions and variable insolation. However, it requires to be further investigated for a broad range/depth of CMC operation, especially for partial shade conditions. Optimising P& O step size and Inc MPPT methods [7, 8] presents employing PSO for grid connected PV systems. This provided approach decreases the settling time, increasing the system's effectiveness. However, the output power oscillates significantly even at a stable state. A multi MW grid-linked solar power system with battery ESS has been suggested in [9]. A technique to sizing for huge ESS are needed for multi-MW solar PV installations to provide dispatchable electricity. Ratings for energy are computed to be excessive, and even if using batteries would not be currently practical for this reason. An

enhanced MPPT and a grid enabled PV system with FCS & MPC have been presented in [10]. Even in partially darkened conditions, the suggested control is capable of tracking the MPP. However, the input power is insufficient to guarantee a quick charging of input capacitance. The least amount of regulation loops and converters for a combination of PV-Wind-BESS with FC and electrolyser has been proposed in [9]. By omitting the PV converter, the suggested hybrid system offers a practical method for incorporating PV into a hybrid system [11]. Nevertheless, this power is unfavourable when there is minimal solar intensity or wind speed, indicating that BESS is intended to pump this negative power into the DC link.

Generally, the inverters manage is used to pass the electricity through the system and connect to the grid, so they are considered the heart of the solar PV plant. Centralised PV inverter technology is being deployed economically to build huge scale solar power installations during the last few decades [12]. However, owing of the centralised MPPT control, these have reduced power ratings and more efficiency losses. With the aim to achieve increased power and voltage levels, multilevel inverters are being adopted to replace the two level inverters present in PV systems [13, 14]. The implementation of three level NPC inverters for solar power systems is made possible by their market accessibility and easy design. However, NPC structure necessitates a common DC link, which lessens its modularity and MPPT control effectiveness [15-17]. Additionally, a foremost difficulty for grid applications is an excess amount of clamping diodes with a rise in the quantity of levels. For improved flexibility, greater adeptness, power utilisation, and power levels, unique modular designs of outstanding performance PV inverters are needed. Two primary topologies of MLIs, namely Modular Multilevel Converter (MMC) MLI and Cascaded H-bridge (CHB) MLI, stand forward as better choices because they combine all the specifications of the PV inverter structure with exceptional performance [18-21]. To improve the inconsistency present in the series-parallel connected lithium ion (Li-Ion) cells, a cell balancing scheme based on switch-matrix and forward converter with active clamp driver topology is presented. This cell balancing scheme is based on transferring the energy from the over-charged cell to auxiliary battery and from auxiliary battery to less charged cell [22, 23]. The primary choices in those applications are high strength factor, and coffee harmonics. The input line cutting-edge harmonics is decreased and power aspect is high. in order to manipulate the LED brightness a current remarks loop is brought [24-25]. They propose an efficient modular sector variable-step perturb and observe (VSPO) maximum power point tracking algorithm. The proposed algorithm enhances the speed tracking and minimizes oscillations level problems associated with traditional P&O methods, swarm optimization also [26-28]. A detailed comparison of Cascade H-Bridge multilevel inverters (CHB-MLI) are presented in the paper based on number of power devices used, Total Harmonic Distortion [29]. This proposed topology offers high power capability associated with less commutation losses, less total harmonic distortion (THD), and involves a smaller number of switching devices and a smaller number of voltage source in comparison of conventional topologies for 31-Level asymmetric multilevel inverter [30]. This converter is most suitable for applications that demand wide input voltage and load ranges. It can be used as a front-end dc–dc converter that can boost variable low voltage from a power source [battery (home/industrial inverter/industrial UPS application), fuel-cell, or solar-PV] and interface it to a high-voltage dc-link, which typically feeds an inverter [31]. In this, 31-level asymmetric inverter is designed using optimal number of switches which produces higher output voltage levels with low harmonic distortion. The voltage sources used in this multilevel inverter is asymmetric in nature to generate output voltage with reduced distortion [32].

Because of its unique framework, the CHB MLI topology is considered to be one of the multilevel converter family's most promising topologies. Modularity, flexibility and self-regulating operation are features of the CHB MLI. Hence this work uses the 31 level CHB MLI for efficient DC to AC conversion for single-phase grid. The following is an outline of this work's primary contributions:

- Using a High gain modified Luo converter maximises the amount of power that is able to be transferred from a PV system.
- The high amount of power extracted from the PV system through the use of CFP optimized ANFIS based MPPT controller.
- With a PI controller as the efficient mechanism, a 31 level CHB MLI converts a DC supply actively to AC.
- Bidirectional battery converter is implemented to enable bidirectional power flow during the battery charging and discharging operations.
- To verify the functionality of the proposed configuration using MATLAB Simulink.

The remainder of the article is organised as follows: Section 2 provides an explanation of the proposed system. Section 3 establishes the modelling and control of a proposed system. Section 4 shows the system simulation and outcomes. Section 5 contains the conclusion.

2. Proposed System Description

One of the most popular natural resources is solar PV based energy generation. Due to pollution and the decreasing availability of traditional sources of energy, solar energy is becoming more and more popular as an emerging form of renewable energy.

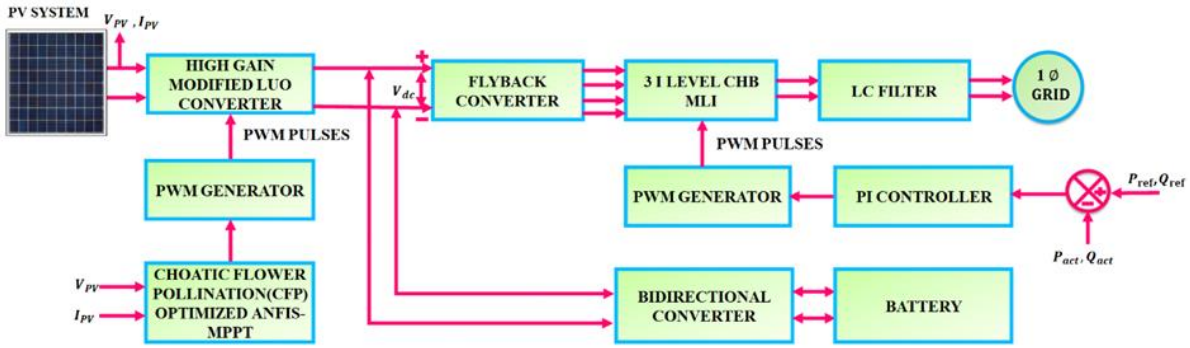

Figure 1. Proposed PV incorporated grid system using CFP optimized PI controller

The most common application of solar energy is to produce PV power. Figure 1 illustrates the schematic diagram of PV incorporated single-phase grid. It contains of a PV panel, Battery, High gain modified Luo converter, CFP optimized ANFIS based MPPT, 31 level CHB MLI and LC filter.

Due to fluctuating nature of PV system, the attained dc output voltage getting poor. With the application of high gain modified Luo converter, the PV dc output voltage is gained with lowered stress and less control-switch complexity. The ANFIS based MPPT controller with CFP optimisation monitors the PV panel's maximum power point and adjusts its operating point to maximise power output. Compared to conventional methods, the proposed CFP-ANFIS based MPPT is capable of tracking the MPP with higher accuracy. The CFP optimised ANFIS controls the dc-link voltage, and by employing this optimisation, the ANFIS controller parameters are tuned optimally. Through a flyback converter, this voltage is transmitted to the 31 level CHB MLI. With a single dc input voltage, this converter is utilised to govern multiple output voltages. The 31 level CHB MLI is convert the dc output voltage into ac output voltage, which is fed to the single-phase power grid. The necessary bidirectional flow of electricity for battery charging and discharging is provided by a bidirectional DC-DC converter. When the PV panel's power generation surpasses the amount of energy needed by the grid, the additional power is applied to recharge the batteries. The additional power is derived from the charged batteries when the PV panels' output is lacking to satisfy the grid's needs. Finally, the resultant AC output voltage is then eliminated from harmonic components injected into the single-phase grid.

3. Proposed System Modelling

3.1 PV System Modelling

PV panel made up of several series connected PV cells that is used to boost the voltage and power produced by a PV system. The voltage of a solar energy system is calculated through combining the voltages of its individual cells, and its power output is calculated through dividing its generated voltage by its supplied current. Figure 2 depicts the electrical setup of a PV cell.

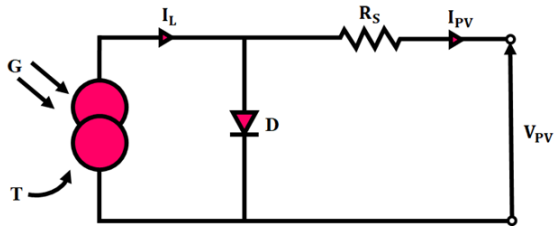

Figure 2. Equivalent circuit of PV panel PI

The equations used for the relationship between the output voltage and current of the PV cell are as follows:

$$I_{PV} = I_L - I_0\left[e^{\frac{q(V_{PV}+I_{PV}+R_S)}{nkt}} - 1\right] \quad (1)$$

$$I_L(G,T) = I_{CC}\frac{G}{100}\left[1 + a(T - T_{ref})\right] \quad (2)$$

$$I_0(T) = I_0(T_{ref}).\left(\frac{T}{T_{ref}}\right)^{\frac{a}{n}}.e^{\frac{-q.Eg}{n}\left(\frac{1}{T}-\frac{1}{T_{ref}}\right)} \quad (3)$$

$$I_0(T_{ref}) = \frac{I_{CC}}{e^{\frac{qV_{OC}}{nkT_{ref}}}-1} \quad (4)$$

$$R_S = \frac{dV_{PV}}{dI_{PV}}|V_{OC} - \frac{nkT}{I_{CC}qe^{\frac{qV_{OC}}{nkT_{ref}}}} \quad (5)$$

where G represents solar irradiation, T represents temperature, K represents the plank's constant, I_0 represents saturation current, I_L represents photocurrent, R_S represents series resistance, R_p represents shunt resistance, I_{PV} denotes PV cell output current, and V_{PV} represents PV cell output voltage. A current source, a series resistance, a diode, and a shunt resistance compose the equivalent circuit model of a PV cell. The output V & I of the PV cell are related by the diode equation, which takes into account solar radiation, temperature, saturation current, and other aspects. The output V and I are reduced, and losses are added by the shunt and series resistances, which also have an effect on the performance of the PV system. The poor dc output voltage of PV panel is enhanced using high gain modified Luo converter, which is explained as follows as.

3.2 High Gain Modified Luo Converter Modelling

This section discusses the High Gain Modified Luo dc-dc converter's design. Figure 3 demonstrates the way the traditional Luo converter has been modified by adding an inductance to the output side, which lessens the strain across the output capacitor. This converter circuit has the benefit of increasing the converter's voltage gain. The switching capacitance-inductor cell, which has three inductors (L_1, L_2 and L_O), three diodes (D_1, D_2 and D_O), and three capacitor (C_1, C_2 and C_O), is used to create the proposed converter. The magnetic coupling of the inductors L_1 and L_2 makes them non-isolated.

Figure 3 (a) shows Proposed High gain modified Luo converter and 3 (b) & 3 (c) shows the Stage1 and Stage 2 of the proposed converter circuit switches during a steady-state phase of the (CCM) and Figure 3 (d) shows the Waveform of proposed converter. There are two different ways that converter switches are able to operate: Stage1 and Stage 2.

Stage 1: ($t_0 - t_1$)

The power switch (S) has been activated (ON) at time (t_0). Here, the two capacitors (C_1, C_2) and two inductors ($L_1$and L_2) together in parallel to the voltage source (V_{in}). The forward mode diodes (D_1,D_2 and D_3) are operating throughout this time, while the reverse-mode diode and inductor ($D_O$and L_O) are operating.

Stage 2: ($t_1 - t_2$)

The switch (S) has been turned off at time (t_1).). Now, the diode and inductor (D_0,L_0) are in series with the capacitor (C_0) and the two capacitors (C_1,C_2), the source voltage (V_{in}), and the two inductors ($L_1$and L_2). The diode and inductor (D_0,L_0) are operating in the forward mode during this time, and the diodes (D_1,D_2 and D_3) are operating in the reverse mode.

At the time of switching ON state :($t_{on} = DT$)

$$V_{in} = V_{L1} = V_{L2} \quad (6)$$

$$V_{in} = V_{C1} = V_{C2} \quad (7)$$

At the time of switching OFF state :($t_{off} = (1 - D)T$)

$$V_{in} - V_{L1} - V_{L2} + V_{C1} + V_{C2} - V_0 = 0 \quad (8)$$

Thus, during the switching (OFF) time, obtained equation is:

$$V_{L1} = V_{L2} = \frac{3V_{in} - V_0}{2} \quad (9)$$

The following equation is the result of applying the voltage second balance concept across the inductors (L_1 and L_2):

$$V_{in}\, DT + \frac{3V_{in} - V_0}{2}(1 - D)T = 0 \quad (10)$$

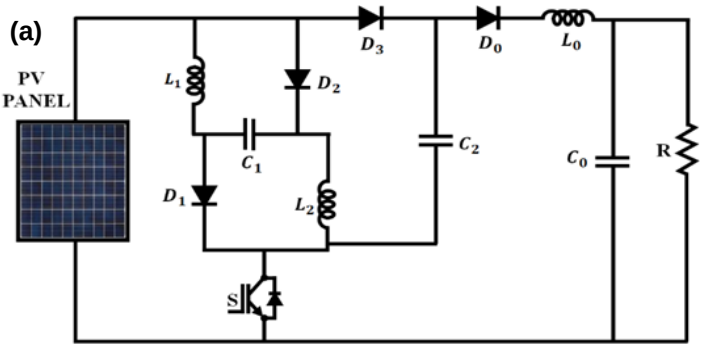

Figure 3(a). Proposed High gain modified Luo converter

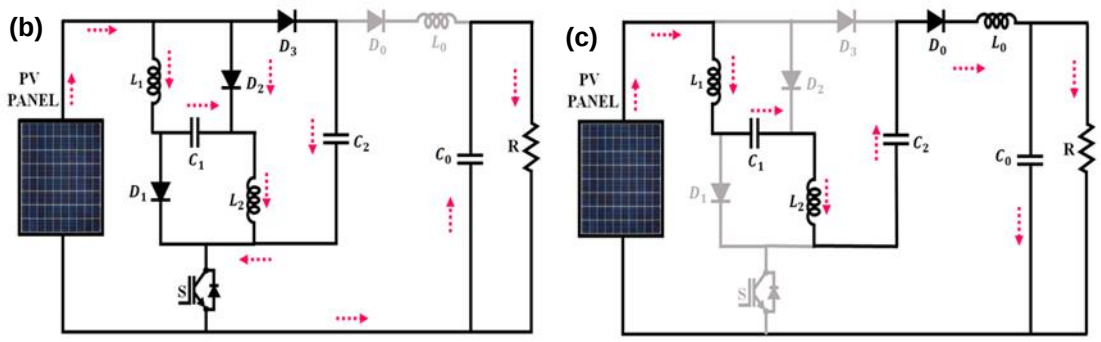

Figure 3 (b) State 1 **(c)** State 2

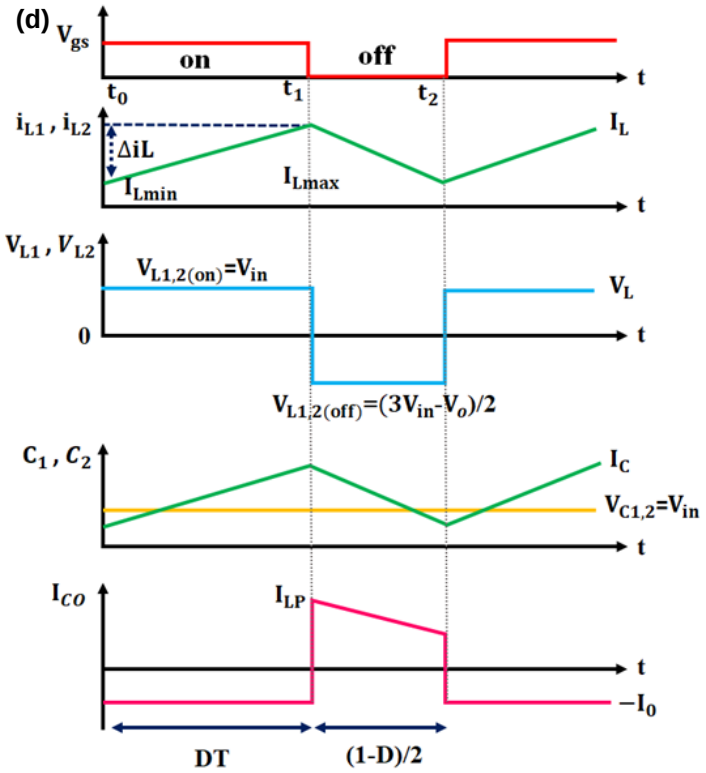

Figure 3(d). Conceptual waveform of proposed converter

As a result, the calculation for the voltage transfer ratio from equation (11) is stated as follows:

$$\frac{V_0}{V_{in}} = \frac{3-D}{1-D} \tag{11}$$

The proposed converter circuit's voltage gain ratio (MD) is

$$M_D = \frac{V_0}{V_{in}} \frac{3-D}{1-D} \tag{12}$$

The input current has been established as follows: For perfect elements, the input and output power have been equivalent.

$$I_{in} = \frac{3-D}{1-D} I_0 \tag{13}$$

The solar cells only have one MPP and nonlinear voltage & current properties. Both the operating point and the MPP are going to alter as soon as these circumstances occur. As a result, a MPPT needs to be employed as a control technique for monitoring the PV system's optimum power generation operating point for various operating situations. This paper uses the CPF optimized ANFIS based MPPT control technique for optimal power tracking, which is explained in the fourth coming section.

3.3 Chaoitic Flower Pollination Optimized Anfis-Mppt Controller ANFIS Based MPPT

The hybrid ANFIS-CFP MPPT algorithm is implemented in the proposed system in order to maximise PV output and provide precise monitoring of utmost power from PV panel. The FLC data is used to train an ANN, which is then optimised using the CFPA approach to reduce the RMSE of both the FLC and the ANN. It includes both FLC and ANN's domination. The FPA method optimises the NN models' threshold and weight to generate the lowest possible RMSE. The entire organisation of hybrid learning, which uses learning data obtained from FLC construction, is shown in Figure 4. Defuzzification, Inference Rule base, and Fuzzification are the fundamental components of the FLC architecture. Fuzzification is the process of transforming real data into linguistic parameters. The employed membership function values of ANFIS controller is represented in Figure 5. The fuzzy inference rule, applied through max min composition, introduces the necessary output. The defuzzification procedure transforms the linguistic parameters into actual values using the centroid method. The parameters utilised in FLC and ANN are shown in Table 1. The subsequent 4 rules form the basis of the entire procedure. The error of fuzzy (E) and error change (dE/CE) input are calculated using the min & max composition (Mamdani's rule) as,

$$E(r) = \frac{dP_{PV}(r)}{dV_{PV}(r)} \tag{14}$$

$$DE = E(r) - E(r-1) \tag{15}$$

$$\mu_{p\to Q}(xy) = \min\left[\mu_p(x), \mu_Q(x)\right], \quad \forall P \in X, \forall Q \in \tag{16}$$

where, $\mu_p(x) = P$ fuzzy membership function of X globe. $\mu_Q(x)$ is Q fuzzy membership function of Y globe where x and y are variables established, respectively.

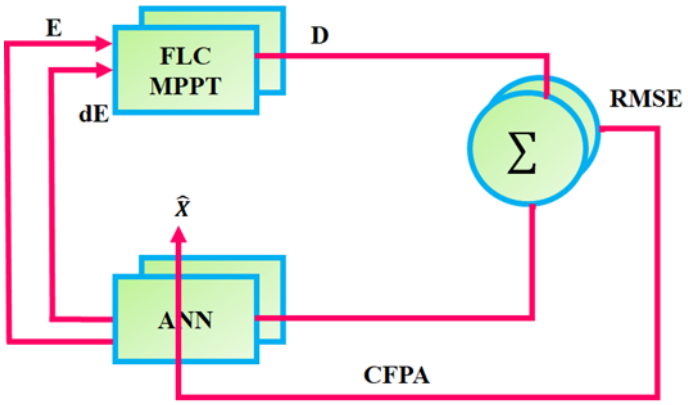

Figure 4. Architecture of CFP optimized ANFIS based MPPT

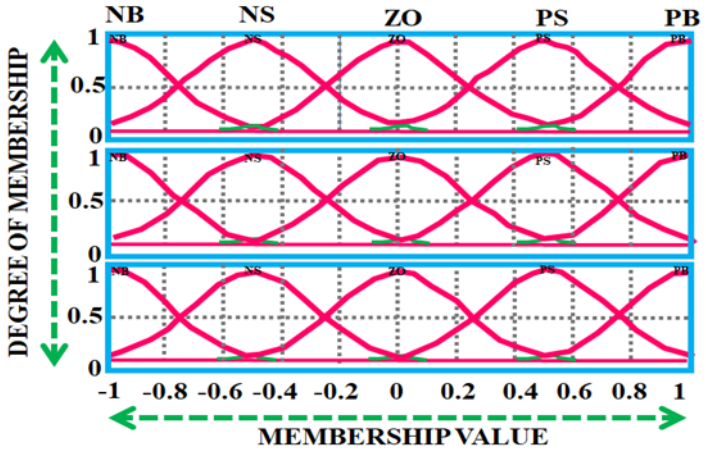

Figure 5. Membership values of employed ANFIS

Table 1. Variables utilised in ANN and FLC

S.No	Parameters	Values
1	Total Neural Network Training Data Sets	200
2	Total Layer (Neural Network)	5
3	Types of Membership Function	Gaussian Type
4	Total Number of Epoch	740
5	Total Fuzzy Rule Base Fired	25

The output D is estimated as:

$$\widehat{D} = D \in \frac{S \int \mu_D(D) dD}{D \in S \int \mu_D(D)} \quad (17)$$

If S is the subarea or globe of discourse and D is the crisp output, $\mu_D(D)$ is the membership function (aggregated), and D is the fuzzy output. Additionally, the formula for the calculation of the neural-fuzzy network output ($\overline{D}$) is,

$$\overline{D} = \mu_A(E) \times \mu_B(dE) \times W_{Li} \quad (18)$$

where W_{Li} = Weight of subsequent ith layer and $\mu_A(E)$ = fuzzy set A membership function in E globe and $\mu_B(dE)$ = fuzzy set B Membership function of in dE globe.

The mathematical formulation of the ANFIS goal function is:

$$RMSE = \left[\frac{1}{P \sum_{i=1}^{P} (D - \overline{D})^2}\right]^{1/2} \quad (19)$$

where, P = whole sample. D = Uncertain output and$\overline{D}$ = the output of a neural network. With the adoption of Chaotic Flower Pollination Optimization (CFPO) algorithm, the ANFIS parameter tuned optimally. The following section gives detailed description proposed CFPO algorithm.

3.3.1 CFPO Algorithm

In addition to being deterministic in nature chaos and randomized numbers indicate unexpected

abnormal behaviours. The natural system's chaos served as the inspiration for metaheuristic techniques, which are close to the chaos order. Large changes in system behaviour result from minor alterations in the chaotic system's starting values. Here, the proposed CFP algorithm fine tunes the parameters ANFIS controller to get optimal results with quick convergence speed.

3.3.2. Flower Pollination Algorithm

FPA is a meta heuristic algorithm, replicates the pollinating process for flowering plants. Pollination of flowers is defined as the movement of flowers pollen. The primary entities involved in this transmission include bats, birds, insects, and other species. These blooms are limited to attracting the birds who are cooperating with one another. Insects such as these are thought to be the primary pollinating agents of flowers.

Four distinct principles of the pollination process, pollination behaviour, and floral constancy are taken into consideration by FPA.

- Rule 1: Whenever a pollinating organism carries pollen, a process known as biotic pollination process take performed. This pollinating process occurs on a global scale and coincides with the Le'vy flights.
- Rule 2: A flower that reproduces on its own without the help of a pollination is said to be abiotic. This process is often to as "local pollinating" since it normally takes less time to move pollen than biotic pollinating accomplishes.
- Rule 3: The ability of pollinating insects to enhance blooming balance advantages specific flower varieties. An expression in mathematics indicating the likelihood of replication is the blossom factor. In accordance to the extent to identical the associated flowers include, the probability rises.
- Rule 4: The kind of pollination is controlled by the potential for a crucial; $p \in [0,1]$. These rules allow the use of both global and local search strategies. By using local search, the finest solutions can be found among those that are already available. Furthermore, the entrapment in a local optimal solution is virtually avoided by global pollination.

It is necessary to modify these rules' equations and for instance, during the stage of global pollination, pollinators like insects transport flower pollen gametes. Since insects are able to fly and cover a larger area, pollen is capable of travelling great distances. Therefore, Eq. 20 is suitable to statistically describe Rule 1 and floral constancy (Rule 3).

$$x_i^{t+1} = x_i^t + \gamma L^{(\lambda)}(g^* - x_i^t)) \quad (20)$$

Here, x_i^t is the ith response vector in the present iteration, and g^* is the optimal solution available for the problem at hand. Here, the scaling factor γ is used to regulate the step size. $L^{(\lambda)}$ is the Le'vy flight step size parameter in essence. Insects have been observed moving in accordance with the Le'vy distributions although while traversing a great distance. Eq. 21 displays the mathematical formula of Le'vy.

$$L \sim \frac{\lambda\Gamma\left(\frac{\lambda\pi}{2}\right)}{\pi}\frac{1}{s^{1+\lambda}} \ (s>>s_o > 0) \quad (21)$$

Here, s is the step size and $\Gamma(\lambda)$ is the common gamma function. For larger steps $s > 0)$ this distribution is applicable. Although $s_o \gg 0$ needs to be in theory, it is possible for s_o to be as low as 0.1 in practise. Eq. 22 illustrates Rules 2 and 3 for local pollination.

$$x_i^{t+1} = x_i^t + \varepsilon\left(x_j^t - x_k^t\right) \quad (22)$$

In Eq. 22, x_j^t and x_k^t are two randomly chosen solutions and $\varepsilon \in [0,1]$ is a kind of pollen from several blooms of identical plants. The use of Levy distribution to search a large number of solution points in the space of search is the method's key feature for optimisation. The algorithm's optimisation logic involves locating solution points across vast distances using a biotic pollination approach inspired by flowers and investigating the area around solution points using an abiotic pollination model.

Algorithm 1. The code of CFPA algorithm

1. Objective function $f(x), x(x_1, x_2, \ldots . x_n)^T$
2. Generate a random initial population. (n: Pollen number)
3. Calculate the best solution for the initial poplation. g^*
4. Probability key $p \in [0, 1]$
5. While t< maximum iteration number do
6. for i=1: n do
7. if r(chaotic map) $<$ p then
8. Global pollination $x_i^{t+1} = x_i^t + \gamma L^{(\lambda)}(g^* - x_i^t))$
9. else
10. Local pollinat $x_i^{t+1} = x_i^t +$ r (Chaotic Map) $(g^* - x_i^t))$
11. end if
12. Evaluate new solutions.
13. Update better solutions in the population
14. end for
15. Choose the best solution g^*
16. end while

Chaotic-based approaches substitute randomised generators in numerous circumstances in order to improve stochastic search capabilities. As a result, the

created Chaotic-FPA method is produced by varying the rand and epsilon variables in the framework using chaotic map functions. The possible values for the rand and epsilon parameters in the formula are logistic, tent, henon, sinus, and tinker bell. Chaotic map functions with variables in the range [0, 1]. Algorithm 1 presents the developed Chaotic FPA Algorithm. The adoption of CFP optimized ANFIS-MPPT algorithm, the maximum power extracted from the PV system with high tracking efficiency.

3.4 Fly-Back Converter Modelling

The Flyback converter (FBC) with an R load is shown in Figure 6. The FBC, which divides an inductor in half to create a transformer and enable isolation of electricity between the i/p and o/p, is the device that began it all. Its size is minimal when compared to the essential transformer.

The output power of flyback converters is used for high voltage power sources for TVs and computer monitors. With few elements, it provides varied functionality. For instance, to boost the power by including windings, diodes, and capacitors. The voltage across the transistor is equal to the addition of the reproduced load voltage V/n and the DC reference voltage Vg. Sounds connected to the transformer's leakage inductance can occasionally be the source of the extra volume.

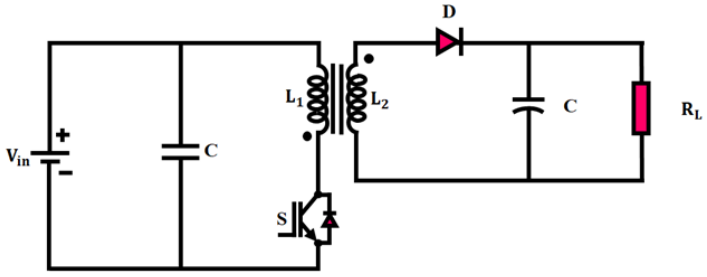

Figure 6. Flyback converter

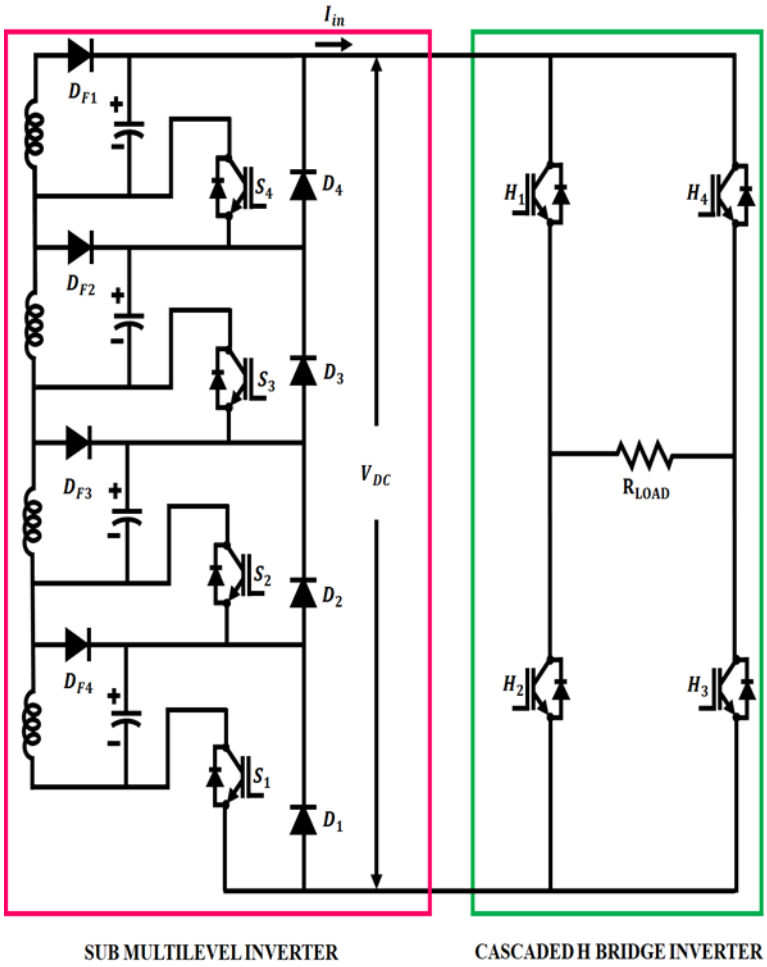

Figure 7. 31- level CHB MLI

It are potentially necessary to use a trigger circuit to lower the visible voltage's magnitude to an appropriate value that is still within a transistor's maximum voltage tolerance.

When employing the mean-shift methodology, there are two ways of expressing a flyback converter. The initial approach entails moving the stack back to the critical side, followed by the substitution of PWM switches and linear analogues for the IGBT and diodes.

3.5 31 Level CHB MLI Modelling

MLI is frequently utilised in applications requiring high and medium power. Three distinct MLI types include the Cascaded H-Bridge (CHB), the Neural Point Clamped (NPC), and the Flying Capacitor (FC) Inverters. Regarding these types of topologies, the CHB inverter is preferred due to its simple appearance, adaptability, and capacity to work with clean sources of energy. Asymmetrical and symmetrical CHB inverters are distinguished by the size of the dc voltage source, respectively. In a symmetrical CHB MLI, the supply voltage source maintains identical magnitude. The output voltage is capable of reaching "M" levels if there's "N" linked H-bridges, whereby M=2N+1 is the total amount of levels. As a result, a symmetrical CHB MLI uses fifteen H-bridges to create an output voltage waveform with 31 levels. In the asymmetry CHB MLI, the combination of magnitudes (input dc voltage source) is supplied as $V_{dc1}:V_{dc2}:V_{dc3}:V_{dc4} = 1:2:4:8$ and is employed to produce 31 levels. Therefore $,M = (2Nx2) - 1$ is an expression for asymmetrical MLI. Where N is the number of Hbridges and M is the highest level (in the output voltage waveform).

Only 8 MOSFET switches and 4 power diodes are required to create a 31-level output waveform from an asymmetrical CHB MLI as shown in Figure 7. Asymmetrical design is therefore preferred since it uses fewer parts to provide larger peak voltage levels. As a result, switching losses are drastically decreased. The input voltages are $V_{dc1} = 13V, V_{dc2} = 26V, V_{dc3} = 52V, V_{dc4} = 104V$. As a result, the following Table 2 provides the inverter output voltage. The logic gate circuit receives the sine and dc offset waves, which form switching pulses for gates that produce PWM for the switches.

3.6 Bidirectional Battery Converter Modelling

The process of converting energy in the bettery system requires an uninterrupted supply of electrical energy. The control system makes use of the DC to DC bidirectional chopper to accomplish this goal. The design of the converter under discussion is shown in Figure 8.

Table 2. Switching table of 31-Level CHB MLI

Inverter V_{output}	S_4	S_3	S_2	S_1	H_1	H_2	H_3	H_4
15 V_{dc}	1	1	1	1	1	1	0	0
14 V_{dc}	1	1	1	0	1	1	0	0
13 V_{dc}	1	1	0	1	1	1	0	0
12 V_{dc}	1	1	0	0	1	1	0	0
11 V_{dc}	1	0	1	1	1	1	0	0
10 V_{dc}	1	0	1	0	1	1	0	0
9 V_{dc}	1	0	0	1	1	1	0	0
8 V_{dc}	1	0	0	0	1	1	0	0
7 V_{dc}	0	1	1	1	1	1	0	0
6 V_{dc}	0	1	1	0	1	1	0	0
5 V_{dc}	0	1	0	1	1	1	0	0
4 V_{dc}	0	1	0	0	1	1	0	0
3 V_{dc}	0	0	1	1	1	1	0	0
2 V_{dc}	0	0	1	0	1	1	0	0
1 V_{dc}	0	0	0	1	1	1	0	0
0 V_{dc}	0	0	0	0	0	0	0	0
-1 V_{dc}	0	0	0	1	0	0	1	1
-2 V_{dc}	0	0	1	0	0	0	1	1
-3 V_{dc}	0	0	1	1	0	0	1	1
-4 V_{dc}	0	1	0	0	0	0	1	1
-5 V_{dc}	0	1	0	1	0	0	1	1
-6 V_{dc}	0	1	1	0	0	0	1	1
-7 V_{dc}	0	1	1	1	0	0	1	1
-8 V_{dc}	1	0	0	0	0	0	1	1
-9 V_{dc}	1	0	0	1	0	0	1	1
-10 V_{dc}	1	0	1	0	0	0	1	1
-11 V_{dc}	1	0	1	1	0	0	1	1
-12 V_{dc}	1	1	0	0	0	0	1	1
-13 V_{dc}	1	1	0	1	0	0	1	1
-14 V_{dc}	1	1	1	0	0	0	1	1
-15 V_{dc}	1	1	1	1	0	0	1	1

Two controlled toggle switches, S_a and S_b, an inductive element, L_d and a capacitor that serves as a filter, C_d make up the DC to DC converter. The converter ought to be thought of as a combination of two basic electrical chopping circuits: a step-down chopper and a step-up chopper. The bidirectional DC/DC converter enables both energy phase and regeneration mode operation when the battery is being recharged. It is produced by a suitable control mechanism, leading to two signals that act as control for the converter's-controlled transistor switches. The battery's electrical power storage is controlled using a bidirectional DC/DC converter's control system. During this converter's control, the proper procedures for the battery bank's release and charging have been developed.

4. Results and Discussion

Grid connected PV system using high gain modified luo converter with CFP optimized MPPT and 31 level CHB MLI presented in this work. The MATLAB simulation platform is implemented to validate the overall performance of the system. From the obtained simulation findings, is it observed that the proposed system achieves highest efficiency value of 94.5% with minimized THD value. Table 3 represents the parameter specifications of proposed system.

The PV panel waveforms are depicted in Figure 9, in which temperature waveform of solar panel is depicted in Figure 9(a), which details that initially temperature is sustained at 25℃, after 0.3s there is a rise in temperature of 35℃ and maintained constant throughout the system. Irradiation waveform of solar panel shown in Figure 9(b), details that 800 W/sq.m of irradiance is maintained in the beginning and it is raised to 1000 W/sq.m after 0.3s, which is sustained constantly throughout the system. Initially solar voltage is maintained at 58V till 0.3s and it is raised to 70V after 0.3s which is constantly maintained throughout the system as depicted in Figure 9(c). In the beginning, there is a sudden raise in current above 20A as shown in Figure 9 (d), which is dropped below 10A and maintained constantly at 12A after 0.3sec.

The output voltage and current waveforms of converter is presented in Figure 10, which the converter voltage is raised initially above 350V and it is maintained constant at 300V after 0.2s which is maintained constant throughout the system as displayed in Figure 10(a).

In the beginning, there is a sudden rise in current above 3A which is then decreased and maintained constant at 0.5A with minor distortion as depicted in Figure 10(b).

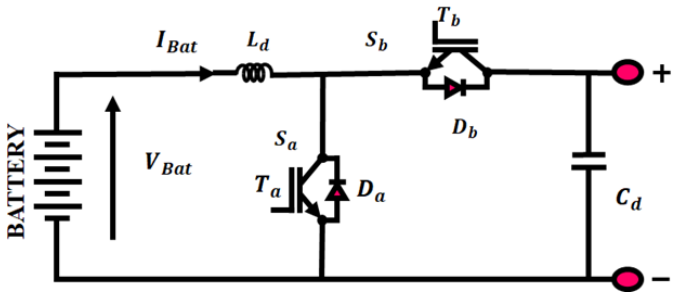

Figure 8. Bidirectional Battery Converter

Table 3. Parameter Specifications

Parameters	Descriptions
PV System	
Short Circuit Current	8.3A
Peak power	$10KW$, 10 Panels
Series Connected solar PV Cells	36
Open Circuit Voltage	12V
High Gain Modified Luo converter	
$L_1L_2L_o$	$1.2\ mH$
C_{in}	$4.7\mu F$
C_o	$200\ \mu F$
Switching Frequency	10KHz

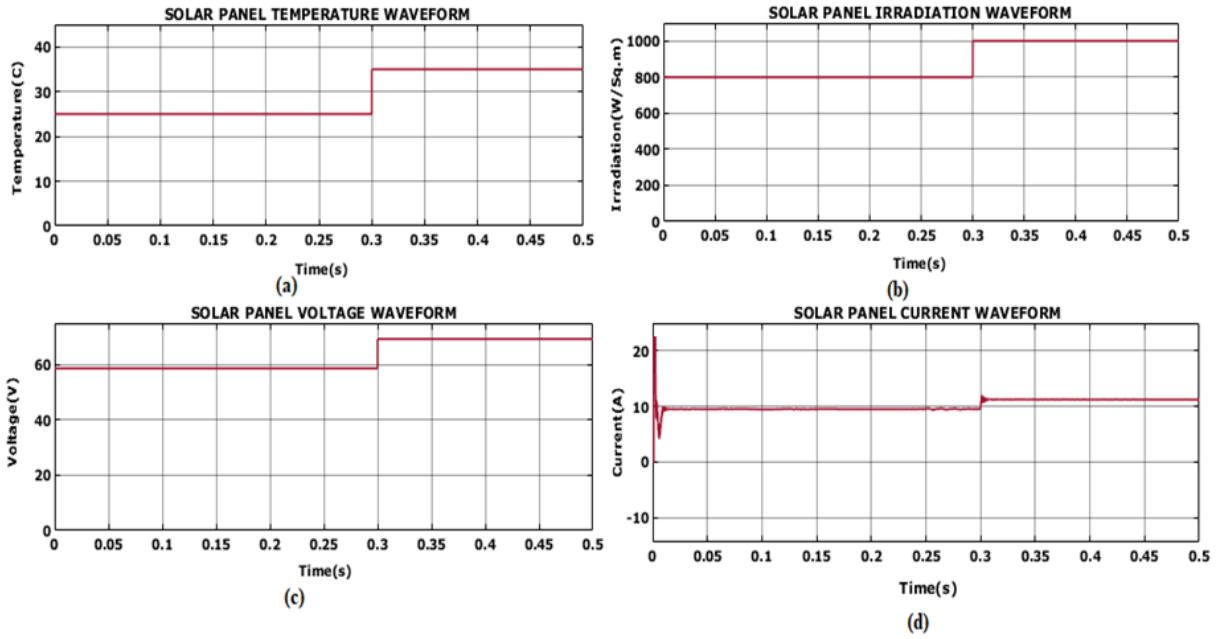

Figure 9. Solar panel waveforms (**a**) Temperature (**b**) Irradiation (**c**) Voltage (**d**) Current

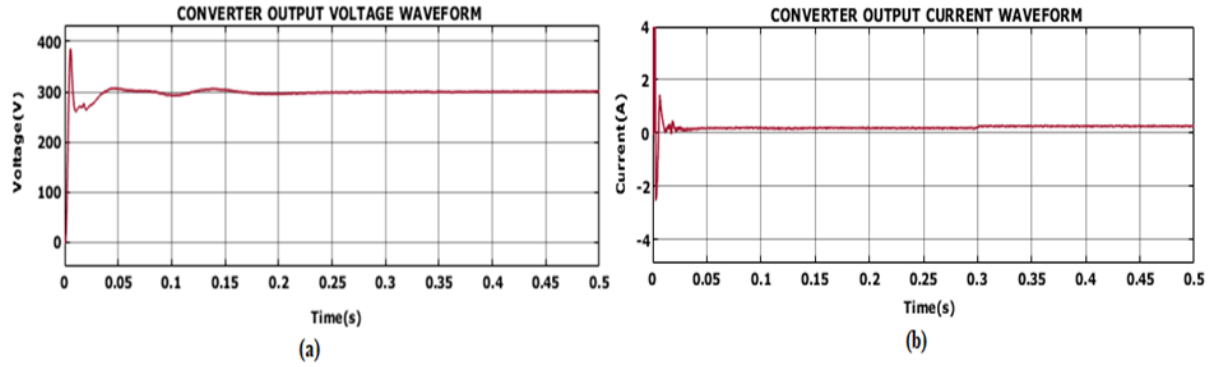

Figure 10. Converter waveforms (**a**) Voltage (**b**) Current

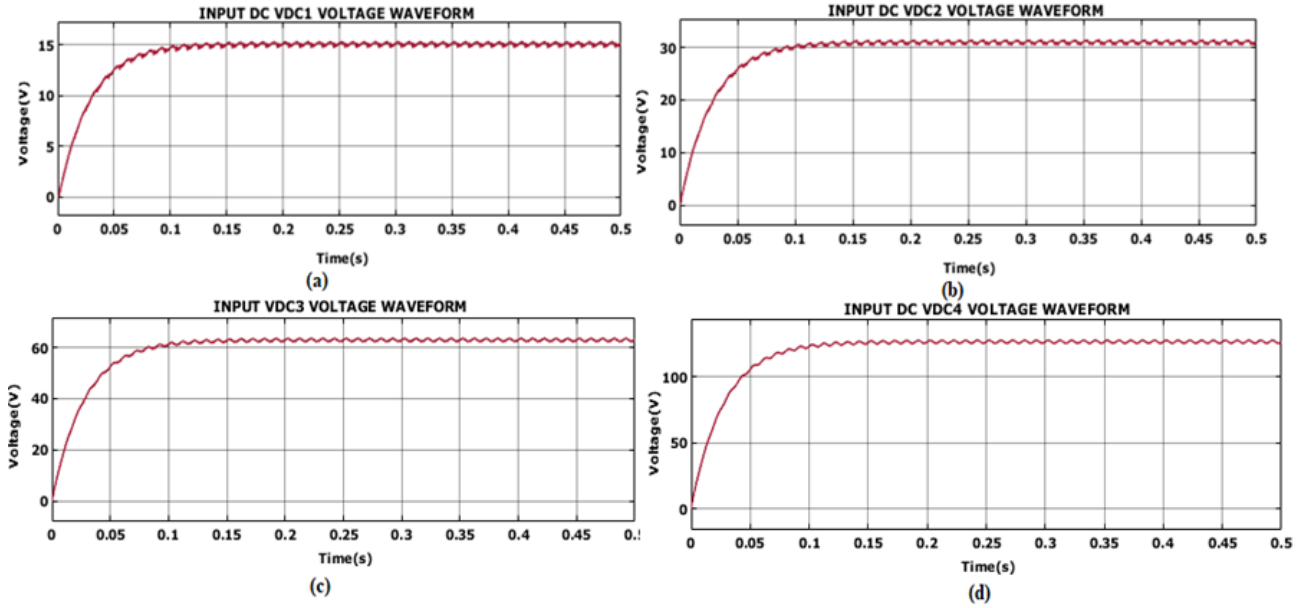

Figure 11. Input DC voltage waveforms (a) V_{DC1} (b) V_{DC2} (c) V_{DC3} (d) V_{DC4}

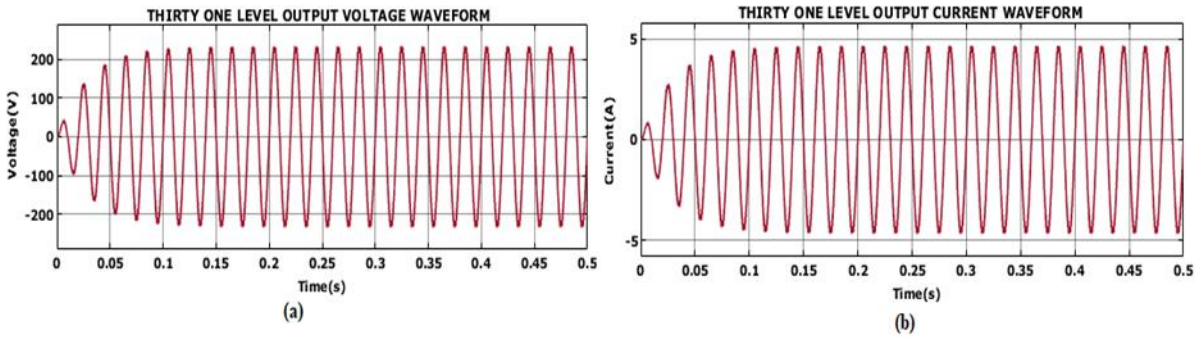

Figure 12. Output waveform for 31-level inverter (**a**) Voltage (**b**) Current

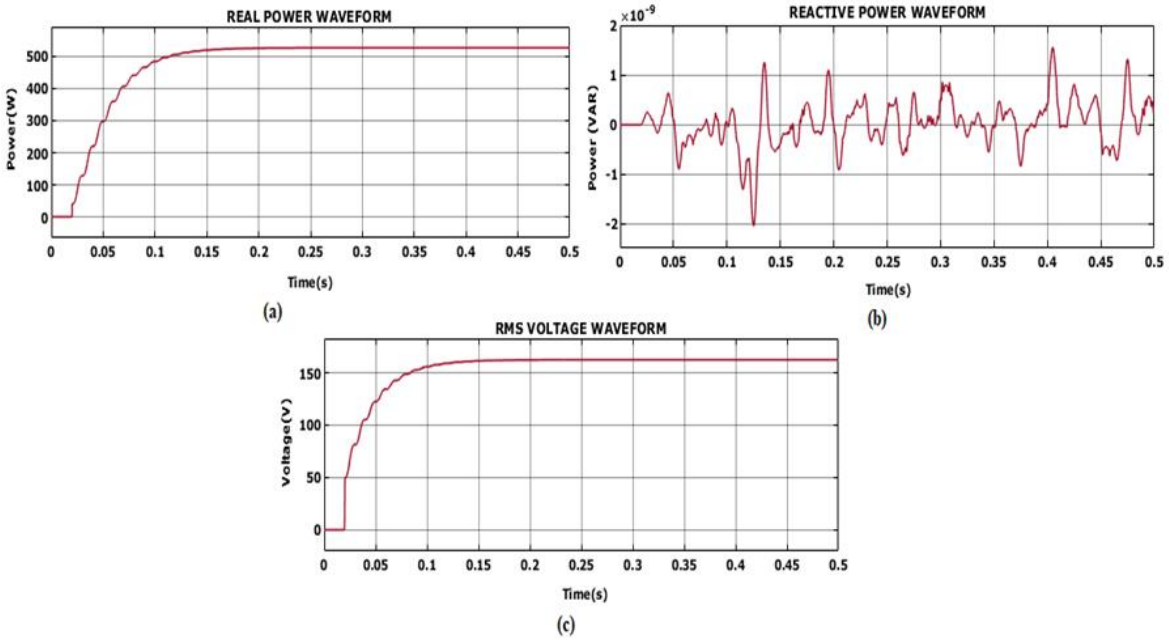

Figure 13. Grid waveforms (**a**) Real power (**b**) Reactive power (**c**) RMS voltage

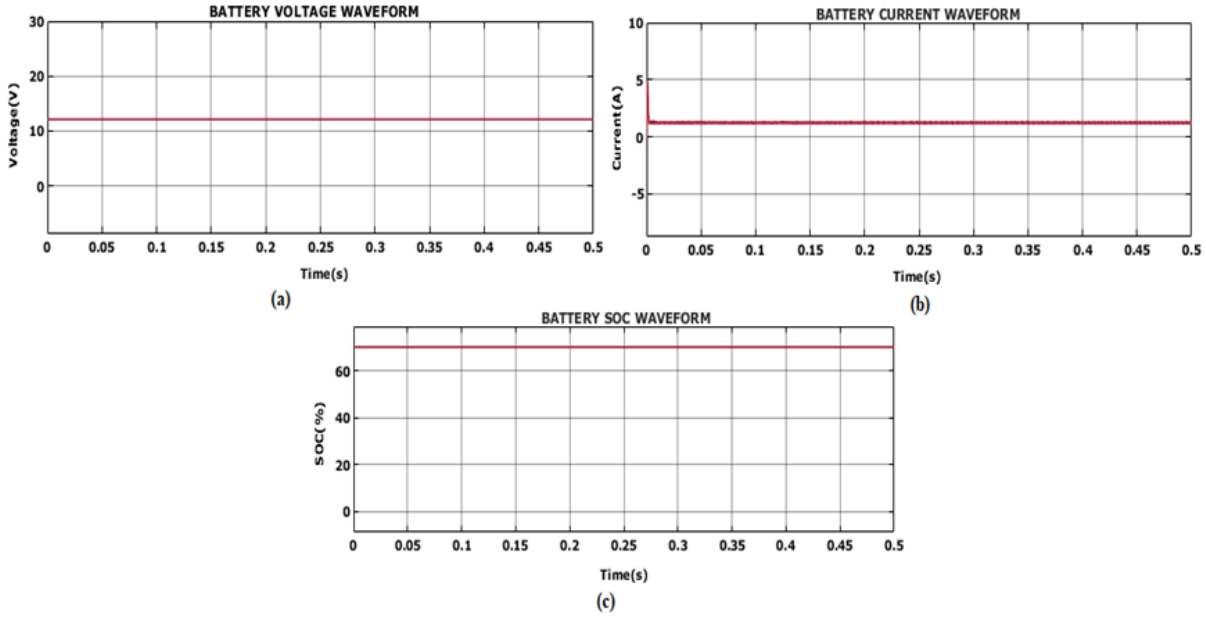

Figure 14. Battery waveforms (**a**) Voltage (**b**) Current (**c**) SOC

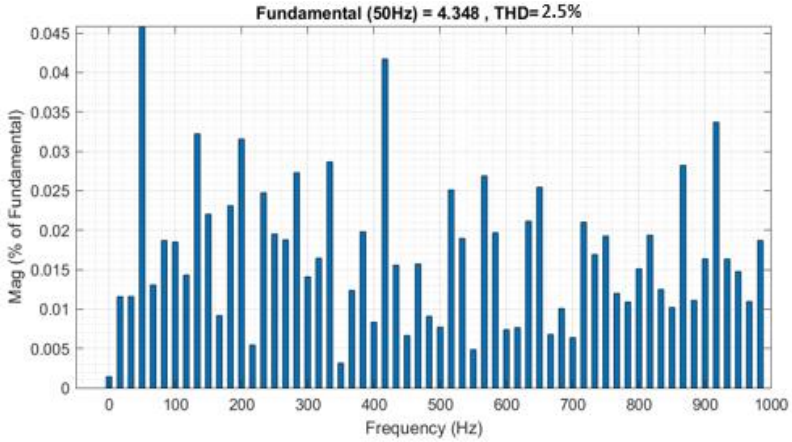

Figure 15. THD waveform

Converters	Efficiency (%)
In ref [23]	75
In ref [24]	80
SEPIC [25]	88.82
Luo [26]	90
High Gain Modified Luo converter	94.5

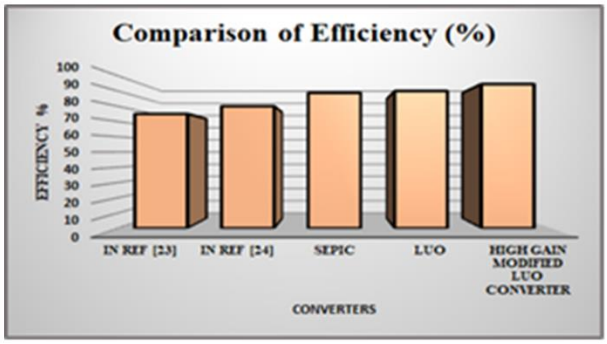

Figure 16. Efficiency Comparison

The input DC voltage waveforms are depicted in Figure 11, which DC input voltage V_{DC1} is shown in Figure 11(a), details that voltage is gradually raised to 15V and maintained constant with minor distortions. Figure 11(b) details that input DC voltage V_{DC2} is gradually increased and maintained constant above 30 V with reduced distortion in the waveforms. The input DC voltage V_{DC3} is illustrated in Figure 11(c), details that voltage is slowly raised and maintained constant above 60V with fewer distortions. The voltage waveform for V_{DC4} is displayed in Figure 11(d), which details that voltage is constantly maintained at 150V with lesser distortion after gradually raise in the beginning.

The waveforms for output voltage and current of 31-level inverter is represented in Figure 12, in which voltage is maintained constant and varies between the range of $\pm 230V$ throughout the system as shown in Figure 12 (a). The output current waveform for 31-level inverter is depicted in Figure 12(b), details that inverter current is maintained constant and varies within the limit of $\pm 4A$ throughout the system. The waveforms for grid showing real power, reactive power and RMS voltage are depicted in Figure 13. The stable real power and reactive power is obtained, which is illustrated in Figure 13 (a) & (b) respectively. The RMS voltage waveform shown in Figure 13(c) details that voltage is gradually raised and maintained constant at 170V throughout the system.

The battery waveforms are depicted in Figure 14, in which battery voltage is sustained at 12V throughout the system as shown in Figure 14 (a). The current waveform for battery is shown in Figure 14 (b), in which current is maintained constant at 2A throughout the system. Figure 14 (c) illustrates battery SOC waveform, in which 70% of charge is held in battery. The proposed system obtains the reduced THD value of 2.5% as illustrated in Figure 15.

4.1 Comparison Analysis

As shown in Figure 16, the efficiency of the proposed converter is compared favourably to that of the other popular converters. Given that it achieves an efficiency of 94.5%, it confirms that the proposed converter's efficiency is far higher than that of other converters. Thus, it is established that the presented converter performs consistently much better than the existing methods. Similar to this, the MPPT tracking efficiency is significantly enhanced by the application of CPF optimised ANFIS based MPPT, which, as demonstrated in Figure 17, attains an efficiency value of 98%. Compared to the controllers' efficiency values published in this proposed controller has high efficiency [25-27]. The evaluation of the proposed 31 level CHB MLI with various level inverters, comprising 5, 9, 11, 31 level asymmetrical CHB MLI and PM-SCHM is shown in Figure 18. The below graph shows that the proposed 31

level CHB MLI resulted in a 2.5% lower THD value than other techniques.

Figure 19 illustrates the comparison of convergence speed of proposed chaotic flower pollination algorithm with Flower pollination algorithm. The above graph shows that the proposed CPFA has quick convergence. PV systems are highly recommended for complex applications where output power variations are expected. They are well known for their lightning-fast convergence, extraordinary precision, and ability to forecast PV cell nonlinearities in the face of rapidly changing meteorological conditions without incurring local MPP under-tracking problems.

MPPT	Tracking Efficiency (%)
P&O [27]	90.5%
INC [28]	96%
Fuzzy [29]	97.79%
CFP-ANFIS based MPPT	98 %

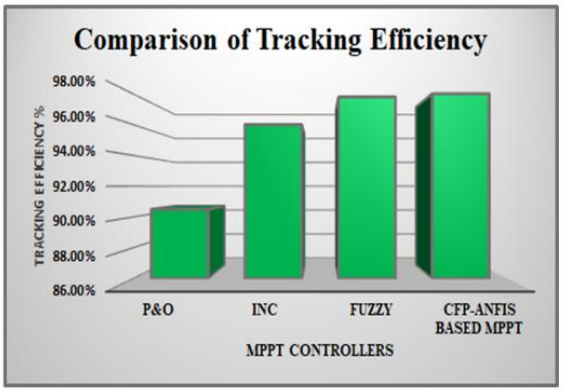

Figure 17. Tracking Efficiency Comparison

MLI TOPOLOGY	THD%
5-Level CHB MLI [30]	20.64%
9-Level CHB MLI [30]	15.17%
11-Level CHB MLI [30]	14.44%
PM-SCHM [21]	16.49%
31-Level Asymmetrical Multilevel [31]	3.95%
31- Level Asymmetrical MLI [32]	3.35%
Design of 31-level Asymmetric [33]	3.20%
31-Level asymmetrical CHB [10]	3.06%
Proposed 31- Level CHB MLI	2.5%

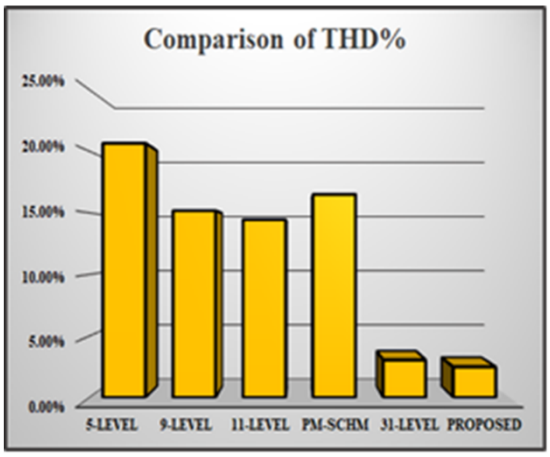

Figure 18. THD Comparison

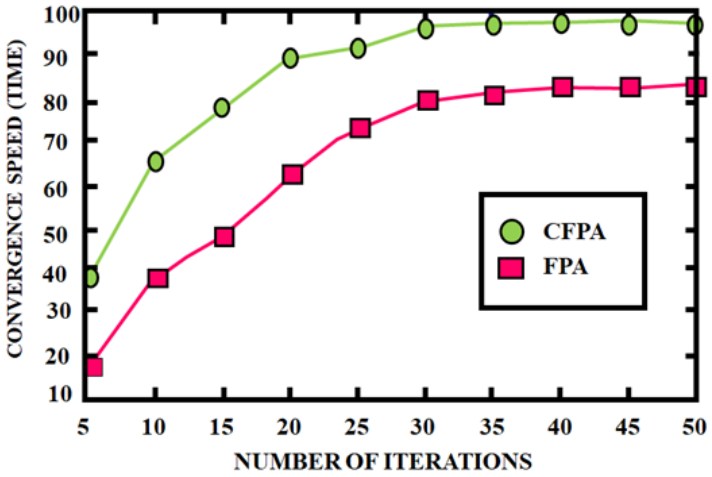

Figure 19. Convergence speed

5. Conclusion

By integrating a PV system that is efficiently controlled by a CFP-optimized ANFIS-based MPPT controller suitable for maximising performance in the face of continuously changing weather conditions, the current study advances the field of green energy integration. Adopting the High Gain Modified Luo Converter makes a big difference in the PV system's effort to achieve maximum efficiency. Furthermore, the scope of this study is expanded to encompass a bidirectional converter linked through a common DC link to an energy storage device, like a battery. After that, the Flyback Converter receives the output power and is seamlessly connected to a 31-level CHB MLI that is managed by a PI controller. The efficient power delivery to the grid made possible by this sturdy inverter design facilitates the controlled and smooth integration of renewable energy sources. The overall performance of the system is verified using the MATLAB simulation environment. The suggested strategy delivers the highest efficiency with the lowest THD value of 2.5% and 94.5%, respectively, based on the results of the simulation. The major scope of the future work is hardware implementation of high power 31-level CHB MLI.

References

[1] K.S. Kavin, P. Subha Karuvelam, Abhinav Pathak, T.R Premila, R. Hemalatha, Tharwin Kumar, Modelling and Analysis of Hybrid Fuzzy Tuned PI Controller based PMBLDC Motor for Electric Vehicle Applications. SSRG International Journal of Electrical and Electronics Engineering, 10(2), (2023) 8-18. https://doi.org/10.14445/23488379/IJEEE-V10I2P102.

[2] K.S. Kavin, P. Subha Karuvelam, PV-based Grid Interactive PMBLDC Electric Vehicle with High Gain Interleaved DC-DC SEPIC Converter. IETE Journal of Research, 69(7), (2023) 4791-4805. https://doi.org/10.1080/03772063.2021.1958070

[3] A. Kumar, V. Verma, Performance enhancement of single-phase grid-connected PV system under partial shading using cascaded multilevel converter. IEEE Transactions on industry applications, 54(3), (2018) 2665-2676. https://doi.org/10.1109/TIA.2017.2789238

[4] Y. Lu, K. Sun, H. Wu, X. Dong, Y. Xing, A three-port converter based distributed DC grid connected PV system with autonomous output voltage sharing control. IEEE Transactions on Power Electronics, 34(1), (2018) 325-339. https://doi.org/10.1109/TPEL.2018.2822726

[5] Y.S. Perdana, S.M. Muyeen, A. Al-Durra, H.K. Morales-Paredes, M.G. Simoes, Direct connection of supercapacitor–battery hybrid storage system to the grid-tied photovoltaic system. IEEE Transactions on Sustainable Energy, 10(3), (2018) 1370-1379. https://doi.org/10.1109/TSTE.2018.2868073

[6] M.H. Ibrahim, S.P. Ang, M.N. Dani, M.I. Rahman, R. Petra, S.M. Sulthan, Optimizing Step-Size of Perturb & Observe and Incremental Conductance MPPT Techniques Using PSO for Grid-Tied PV System. IEEE Access, 11, (2023) 13079-13090. https://doi.org/10.1109/ACCESS.2023.3242979

[7] R. López-Erauskin, A. Gonzalez, G. Petrone, G. Spagnuolo, J. Gyselinck, multi-variable perturbs and observe algorithm for grid-tied PV systems with joint central and distributed MPPT configuration. IEEE Transactions on Sustainable Energy, 12(1), (2020) 360-367. https://doi.org/10.1109/TSTE.2020.2996089

[8] V. Rallabandi, O.M. Akeyo, N. Jewell, D.M. Ionel, incorporating battery energy storage systems into multi-MW grid connected PV systems. IEEE Transactions on Industry Applications, 55(1), (2018) 638-647. https://doi.org/10.1109/TIA.2018.2864696

[9] H. Myneni, S.K. Ganjikunta, Energy management and control of single-stage grid-connected solar PV and BES system. IEEE Transactions on Sustainable Energy, 11(3), (2020) 1739-1749. https://doi.org/10.1109/TSTE.2019.2938864

[10] S. Vanti, P.R. Bana, S. D'Arco, M. Amin, Single-stage grid-connected PV system with finite control set model predictive control and an improved maximum power point tracking. IEEE Transactions on Sustainable Energy, 13(2), (2021) 791-802. https://doi.org/10.1109/TSTE.2021.3132057

[11] M.M Gulzar, A. Iqbal, D. Sibtain, M. Khalid, an innovative converter less solar PV control strategy for a grid connected hybrid PV/wind/fuel-cell system coupled with battery energy storage. IEEE Access, 11, (2023) 23245-23259. https://doi.org/10.1109/ACCESS.2023.3252891

[12] H. Katir, A. Abouloifa, K. Noussi, I. Lachkar, A. El Aroudi, M. Aourir, F. El Otmani, F. Giri, Fault tolerant backstepping control for double-stage grid-connected photovoltaic systems using cascaded H-bridge multilevel inverters. IEEE Control systems letters, 6, (2021) 1406-1411. https://doi.org/10.1109/LCSYS.2021.3095107

[13] P.R. Bana, K.P. Panda, S. Padmanaban, L. Mihet-Popa, G. Panda, J. Wu, Closed-loop control and performance evaluation of reduced part count multilevel inverter interfacing grid-connected PV system. IEEE Access, 8, (2020) 75691-75701. https://doi.org/10.1109/ACCESS.2020.2987620

[14] T. Santhosh Kumar, J. Shanmugam, (2020) Design and analysis of CHB inverter by using Pi fuzzy and ANN techniques with grid connected PV System. 2020 IEEE International Conference for Innovation in Technology (INOCON), IEEE, India. https://doi.org/10.1109/INOCON50539.2020.9298260

[15] G. Tahri, Z.A. Foitih, A. Tahri, Fuzzy logic control of active and reactive power for a grid-connected photovoltaic system using a three-level neutral-point-clamped inverter. International Journal of Power Electronics and Drive Systems, 12, (2021) 453. http://doi.org/10.11591/ijpeds.v12.i1.pp453-462

[16] T. Yu, W. Wan, S. Duan, A modulation method to eliminate leakage current and balance neutral-point voltage for three-level inverters in photovoltaic systems. IEEE Transactions on Industrial Electronics, 70(2), (2022) 1635-1645. https://doi.org/10.1109/TIE.2022.3161809

[17] A.M. Noman, K.E. Addoweesh, A.A. Alabduljabbar, A.I. Alolah, Cascaded H-bridge MLI and three-phase cascaded VSI topologies for grid-connected PV systems with distributed MPPT. International Journal of Photoenergy, 2019, (2019). https://doi.org/10.1155/2019/7642919

[18] M.A. Hosseinzadeh, M. Sarbanzadeh, J. Munoz, M. Rivera, C. Munoz, A. Villalon, (2019) New Reduced Switched Multilevel Inverter for Three-Phase Grid-Connected PV System, Performance Evaluation. IEEE International Conference on Industrial Technology (ICIT), IEEE, Melbourne. https://doi.org/10.1109/ICIT.2019.8755112

[19] T.A. Ahmed, E.E. Mohamed, A.R. Youssef, A.A. Ibrahim, M.S. Saeed, A.I. Ali, Three phase modular multilevel inverter-based multi-terminal asymmetrical DC inputs for renewable energy applications. Engineering Science and Technology, an International Journal, 23(4), (2020) 831-839. https://doi.org/10.1016/j.jestch.2019.11.003

[20] R. Venkedesh, R. AnandhaKumar, G. Renukadevi, THD reduction in measurement of H-Bridge multilevel inverter using pulse modulated switching integrated with linear quadratic Regulator. Measurement: Sensors, 24, (2022) 100435. https://doi.org/10.1016/j.measen.2022.100435

[21] V. Ramalingam, A. Radhakrishnan, R. Govindasamy, (2022) Multilevel Inverter Design with Reduced Switches & Thd Using Fuzzy Logic Controller. SSRN.

[22] S. Shah, M. Murali, P. Gandhi, (2018) A Practical Approach of Active Cell Balancing in a Battery Management System. IEEE International Conference on Power Electronics, Drives and Energy Systems (PEDES), Chennai, India. https://doi.org/10.1109/PEDES.2018.8707811

[23] S.W. Lee, K.M. Lee, Y.G. Choi, B. Kang, Modularized Design of Active Charge Equalizer for Li-Ion Battery Pack. IEEE Transactions on Industrial Electronics, 65(11), (2018) 8697–8706. https://doi.org/10.1109/TIE.2018.2813997

[24] P. Javeed, L.K. Yadav, P.V. Kumar, R. Kumar, S. Swaroop, (2021) SEPIC Converter for Low Power LED Applications. In Journal of Physics: Conference Series, IOP Publishing,1818, (2021) 012220. https://doi.org/10.1088/1742-6596/1818/1/012220

[25] S. Sivarajeswari, D. Kirubakaran, Design and development of efficient Luo converters for DC micro grid. The International Journal of Electrical Engineering & Education, 60(1), (2019). https://doi.org/10.1177/0020720919845152

[26] H. Ramadan, A.R. Youssef, H.H. Mousa, & E.E. Mohamed, An efficient variable-step P&O maximum power point tracking technique for grid-connected wind energy conversion system, SN Applied Sciences, 1, (2019) 1-15. https://doi.org/10.1007/s42452-019-1716-5

[27] N.E. Zakzouk, M.A. Elsaharty, A.K. Abdelsalam, A.A. Helal, B.W. Williams, Improved performance low-cost incremental conductance PV MPPT technique. IET Renewable Power Generation, 10(4), (2016) 561-574. https://doi.org/10.1049/iet-rpg.2015.0203

[28] A.K. Raji, D.N. Luta, Fuzzy rule-based and particle swarm optimization MPPT techniques for a fuel cell stack. Energies, 12(5), (2019) 936. https://doi.org/10.3390/en12050936

[29] T. Antalem, C.K. Prasad, A Comparative Investigation of 5-Level, 9-Level and 11-Level Conventional Cascaded H-Bridge Multilevel Inverters by Using Simulink / Matlab. International Journal of Research in Engineering & Technology, 5, (2017) 19-26.

[30] S. Gupta, K.S. Rathore, P. Bansal, (2018) Design and Analysis of a New 31-Level Asymmetrical Multilevel Inverter Topology with Different PWM Techniques. 3rd International Innovative Applications of Computational Intelligence on Power, Energy and Controls with their Impact on Humanity (CIPECH), IEEE, India. https://doi.org/10.1109/CIPECH.2018.8724251

[31] V.K. Goyal, A. Shukla, Isolated DC-DC Boost Converter for Wide Input Voltage Range and Wide Load Range Applications. IEEE Transactions on Industrial Electronics, 68(10), (2021) 9527-9539. https://doi.org/10.1109/TIE.2020.3029479

[32] G.V. Raman, A. Imthiyas, M.D. Raja, L. Vijayaraja, S. Kumar, (2019) Design of 31-level Asymmetric Inverter with Optimal Number of Switches. IEEE International Conference on Intelligent Techniques in Control, Optimization and Signal Processing (INCOS), India. https://doi.org/10.1109/INCOS45849.2019.8951354

Acknowledgement
The Authors appreciate the continuous support of Annamalai University, India.

Authors Contribution Statement
R. Venkedesh: Conceptualization, Investigation, Methodology, Data collection, Writing original draft; R. AnandhaKumar: Conceptualization, Supervision, Validation, Review and Editing; G. Renukadevi: Supervision and Validation, Review and Editing; All the authors read and approved the final version of the manuscript.

Funding
The Authors declare that no funds, grants, or other support were received during the preparation of this manuscript.

Availability of data
Data will be provided upon request.

Conflict of Interest
The Authors report there are no competing interests to declare.

Has this article screened for similarity?
Yes